

Cost-efficient natural apatite–metakaolin supported TiO₂ mesoporous membrane for dye removal applications



Youssef Guesmi^{a,b}, Ibtissem Ounifi^a, Mohamed Khabbouchi^c, Hassen Agougui^{d,e}, Amor Hafiane^a, Miguel A. Rodríguez^{f,*}

^a Laboratory of Water, Membrane and Environmental Biotechnology, Centre of Research and Water Technologies, Technopark of Borj-Cedria, BP 273, 8020 Soliman, Tunisia

^b Research Institute on Mines and Environment (RIME), Université du Québec en Abitibi-Témiscamingue (UQAT), Rouyn-Noranda, QC J9X 5E4, Canada

^c Chemistry Section, Riyadh Municipality Central Area Labs, Riyadh, Saudi Arabia

^d Faculty of Sciences of Gafsa, University of Gafsa, University Campus, Zarroug, 2112 Gafsa, Tunisia

^e Laboratory of Physical Chemistry of Materials, Faculty of Sciences of Monastir, 5019 Monastir, Tunisia

^f I. Cerámica y Vidrio, CSIC, Madrid, Spain

ARTICLE INFO

Article history:

Received 24 July 2023

Accepted 18 October 2023

Available online 6 November 2023

Keywords:

Natural apatite

Metakaolin

Titanium dioxide

UF membrane

Dye

ABSTRACT

The synthesis of a TiO₂-tight ultrafiltration membrane supported on a low-cost ceramic substrate based on metakaolin and natural apatite was proposed in this study. To optimize the substrate composition, three samples were prepared by combining metakaolin and natural apatite with weight ratios of 25:75 (MK25), 50:50 (MK50), and 75:25 (MK75), and then sintered for 2 h at 850, 900, 950, and 1000 °C. The effect of sintering temperature and metakaolin content on the final properties of the prepared samples was studied in terms of microstructure, porosity, and mechanical strength. According to the results, the mechanical strength increased with increasing temperature and metakaolin content, but at the same time, the porosity decreased. MK50 composition and the temperature of 950 °C were chosen as optimal conditions, and the support was prepared by extrusion. The prepared substrate presented a compressive strength of 4.4 MPa, porosity of 33%, and an average pore size of 2.2 µm. To prepare a crack-free ultrafiltration membrane, the deposition of the TiO₂ top layer was favoured over an alumina intermediate layer. The obtained membrane has a pore size of 6.8 nm and water permeability of 5.6 L h⁻¹ m⁻² bar⁻¹. The membrane performance was tested for the removal of cationic and anionic dyes. The ultrafiltration experiments have shown a high removal rate for anionic and cationic dyes. Specifically, it was found that the removal rates of these dyes exceeded 75% without adjusting the pH of the solution.

© 2023 The Authors. Published by Elsevier España, S.L.U. on behalf of SECV. This is an open access article under the CC BY-NC-ND license (<http://creativecommons.org/licenses/by-nc-nd/4.0/>).

* Corresponding author.

E-mail address: mar@icv.csic.es (M.A. Rodríguez).

<https://doi.org/10.1016/j.bsecv.2023.10.002>

0366-3175/© 2023 The Authors. Published by Elsevier España, S.L.U. on behalf of SECV. This is an open access article under the CC BY-NC-ND license (<http://creativecommons.org/licenses/by-nc-nd/4.0/>).

Membranas mesoporosas de TiO₂, soportadas sobre apatita natural y metacaolín, rentables para aplicaciones de eliminación de colorantes

RESUMEN

Palabras clave:

Apatita natural
Metacaolín
Óxido de titanio
Membrana de ultrafiltración
Colorantes

En este estudio se propone la síntesis de una membrana de ultrafiltración de TiO₂ soportada sobre un soporte cerámico de bajo coste basado en metacaolín y apatita natural. Para optimizar la composición del soporte se prepararon tres formulaciones combinando metacaolín y apatita natural en proporciones de peso de 25:75 (MK25), 50:50 (MK50) y 75:25 (MK75), y luego se sinterizaron durante 2 horas a 850, 900, 950 y 1000 °C. Se estudió el efecto de la temperatura de sinterización y el contenido de metacaolín en las propiedades finales de las muestras preparadas en términos de microestructura, porosidad y resistencia mecánica. De acuerdo con los resultados, la resistencia mecánica aumentó con el aumento de la temperatura y el contenido de metacaolín, pero, al mismo tiempo, la porosidad disminuyó. La composición MK50 y la temperatura de 950 °C se eligieron como condiciones óptimas, siendo el soporte preparado por extrusión. El sustrato presentó una resistencia a la compresión de 4.4 MPa, una porosidad del 33% en volumen y un tamaño medio de poro de 2.2 μm. Para preparar una membrana de ultrafiltración libre de defectos, la capa superior de TiO₂ se depositó sobre una capa intermedia de alúmina. La membrana obtenida tiene un tamaño de poro de 6.8 nm y una permeabilidad al agua de 5,6 L.h.⁻¹m.⁻²bar⁻¹. Se evaluó el rendimiento de la membrana para la eliminación de colorantes catiónicos y aniónicos. Los experimentos de ultrafiltración han mostrado una alta tasa de eliminación de colorantes aniónicos y catiónicos. Específicamente, se encontró que las tasas de eliminación de estos colorantes superaban el 75% sin ajustar el pH de la solución.

© 2023 Los Autores. Publicado por Elsevier España, S.L.U. en nombre de SECV. Este es un artículo Open Access bajo la licencia CC BY-NC-ND (<http://creativecommons.org/licenses/by-nc-nd/4.0/>).

Introduction

Rapid industrial development, excessive population growth, and the loss of natural resources have made water contamination one of the most pressing global challenges [1]. In particular, wastewater generated from chemical and textile industries represents about 20% of industrial water pollution [2]. Several conventional technologies have been widely used for textile wastewater treatment, including adsorption, precipitation, biological treatment, coagulation/flocculation, etc. [3,4]. Due to its high-quality output, low energy consumption, and adaptability in system design, membrane separation is acknowledged as one of the most effective methods in water reclamation [5]. A membrane may be described as a semi-permeable barrier that allows some molecules to pass through, while blocking the passage of other molecules relying on its charge, pores size, etc. The properties of such membranes are strongly affected by the manufacturing process and the starting materials. Based on their low cost, uncomplicated manufacturing, and processability, polymeric membranes have been widely used for industrial wastewater treatment, and hence dominated the membrane market [6]. In counterpart, the ceramic membranes showed obvious superiorities in thermal and chemical stability, while still suffering from their relatively high price [7]. This is mainly due to the high manufacturing cost including the price of the starting materials e.g., alumina, zirconia, titania, silica, and their mixture, and the high sintering temperature [8]. To address this issue, recently many natural minerals and industrial wastes

with low-sintering temperatures have been broadly proposed as membrane support [9–11]. In particular, M. Mouiya et al. prepared ceramic membranes from clay and banana peels as natural porogen. The produced samples had a mean pore size of 0.45 μm and water permeability of 550 L.h⁻¹m.⁻²bar⁻¹ after sintering for 2 h at 1100 °C. The prepared membranes were tested for industrial wastewater and showed a high decrease in turbidity (99%) [12]. A variety of Egyptian natural materials were used by D. Rashad et al. to create tubular ceramic membranes. The membranes made from Aswan kaolin exhibited high compressive strength (2 MPa) and showed a permeate flux of 22.9 L/m² h and bacterial removal of 80% [13].

Responding to the tremendous interest in low-cost ceramic membranes, recent papers have been published summarizing the main obtained results in this research framework over the last two decades [14,7,15]. The authors have drawn that in most reported works: (i) the prepared membranes showed sufficient mechanical and chemical strength, and (ii) a total porosity above 30% was reported, which is comparable to traditional ceramic membranes. Additionally, most membranes have pores size between 0.1 and 5 μm in size, making them ideal for micro-filtration applications and frequently employed for treating oil-water emulsions [7,15].

The above review suggests that the management of waste products and the use of abundant and renewable raw materials could be an emerging approach to overcoming the high cost of ceramic membranes. However, more emphasis should be assigned to the preparation of low-cost membranes with an asymmetric structure to respond to a wide range of applications. These challenges could be resolved by optimizing

the synthesis parameters, which include the choice of a better proportion between the unconventional materials, the appropriate shaping method, and the convenient sintering process. The whole process leads to the obtainment of a robust membrane with micro-scale pore structures ensuring high selectivity and sufficient mass transport [16]. In particular, tight ultrafiltration membranes are mesoporous (2–10 nm) membranes that combine the superior permeability of ultrafiltration membranes with the high dye retention rate of traditional nanofiltration membranes [17]. Polymeric tight ultrafiltration membranes are widely studied and showed promising results [18–20]. Up to this time, there exist few studies dealing with ceramic tight ultrafiltration membranes, especially those made with unconventional materials.

The results of our previous study demonstrated that the combination of natural apatite with alpha alumina to create cost-effective ceramic membranes reduced the required final sintering temperature for the ceramic support [21]. However, this approach resulted in diminished mechanical strength, attributed to the variance in refractory characteristics between alpha alumina and natural apatite. In this context, the use of materials exhibiting thermal properties closely resembling those of apatite, such as clay-based materials, could potentially provide a solution to this challenge. For instance, metakaolin has been reported as an efficient material for separation and adsorption applications [22,23].

TiO₂ is recognized as a commonly applied photocatalyst thanks to its non-toxic nature and chemical stability [24,25]. Furthermore, it has been reported that utilizing TiO₂ over a substrate could be a useful method for improving regeneration efficiency [26]. Notably, the immobilization of TiO₂ onto porous membrane supports has been emphasized as an effective approach to address the challenges associated with catalyst recovery and enhance antifouling properties [27,28].

The primary focus of this study is to create cost-effective ceramic substrates utilizing metakaolin and natural apatite as raw materials, with the ultimate aim of assessing their suitability for TiO₂-tight ultrafiltration membranes. The main optimization parameters for substrate preparation will be the sintering temperature and metakaolin concentration in the composition. The feasibility of the deposition of the TiO₂ tight ultrafiltration membranes over the low-cost substrate will be investigated by direct deposition and by deposition over an alumina intermediate layer. The support and membrane characteristics such as total porosity, pore size, morphology, thickness, and water permeation will be analyzed. Additionally, cationic and anionic dyes will be used to assess the produced membranes' capacity to remove dyes.

Materials and methods

Materials

Natural apatite and metakaolin used in this work for manufacturing the porous support were collected from Metlaoui (Southern Tunisia) and Tabarka (Northern Tunisia), respectively. The detailed characterization of both materials was indicated in our previous work [21,29]. Al₂O₃ (Almatis, CTSG10, Specific Surface Area, BET: 13 m²/g, average particle size,

$d_{50} \approx 0.1 \mu\text{m}$) was used for depositing the intermediate layer. Isopropanol (Merck, 99.5%), Tween 80 (Merck), and Titanium (IV) isopropoxide (Merck, 97%) were the main precursors for preparing the filtration layer of the membrane by the sol-gel process.

Methods

The determination of support composition

To choose the suitable composition between the two materials and the adequate sintering temperature for making the membrane support, a preliminary study was performed. This study was conducted with three different mixtures (25/75, 50/50, and 75/25 wt.%) of metakaolin/natural apatite. The different compositions were homogeneously dry-mixed using alumina balls, then, 2.5 g of the each composition was mixed with approximately 0.15 mL of polyvinyl alcohol (PVA) as a binder and axially pressed under a pressure of 4 kg/cm² to form pellets with a diameter of 15 mm and thickness of approximately 10 mm. According to the dilatometric study, the different samples were sintered for 2 h at 850, 900, 950, and 1000 °C with a heating rate of 5 °C/min. Subsequently, the effect of sintering temperature and sample composition on the support properties was investigated. The samples were labelled using the formula MKX-T, where X stands for the percentage weight of metakaolin in the sample and T stands for the sintering temperature.

Synthesis of membrane

Support. The preparation of the tubular supports was carried out with the chosen composition 50/50 (wt.%), apatite/metakaolin. The inorganic powder was firstly dry mixed for 2 h. According to the plasticity study, the ceramic paste was prepared by adding 43 wt.% of water, 0.6 wt.% carboxymethyl cellulose, and 0.5 wt.% polyethylene glycol to the mixture. Then, the paste was left under a humid atmosphere for 12 h to improve its rheological property. The final samples were obtained by extrusion using a homemade piston extruder developed in the Instituto de Cerámica y Vidrio (ICV-CSIC) Madrid. The outer and inner diameters of the tubular supports were 8 and 4 mm, respectively. The samples were dried in air for 48 h and then sintered at 950 °C for 2 h with heating and cooling rates of 2 °C/min.

Ultrafiltration membrane. To obtain the tight ultrafiltration membranes, the TiO₂ active layer was coated over the prepared supports through two methods. The direct method refers to the coating over the substrate (system 1). While the second method corresponds to the deposition of the TiO₂ over an intermediate layer of α -Al₂O₃ earlier deposited on the supports (system 2). The intermediate and active layers were formed by the dip-coating method. The intermediate layer was performed using 4 wt.% of alumina slurry mixed with 1 mL of Optapix paf-35 as a binder for 100 mL of the dipping solution. Then the mixture was stirred for 2 h and transferred to an ultrasound bath to remove the air bubbles. The coating layer was deposited on the outer surface of the support as follows: one of the support ends was closed and introduced vertically into the suspension. After a dipping time of 40 s, the support was withdrawn at a constant velocity around 2 cm/s.

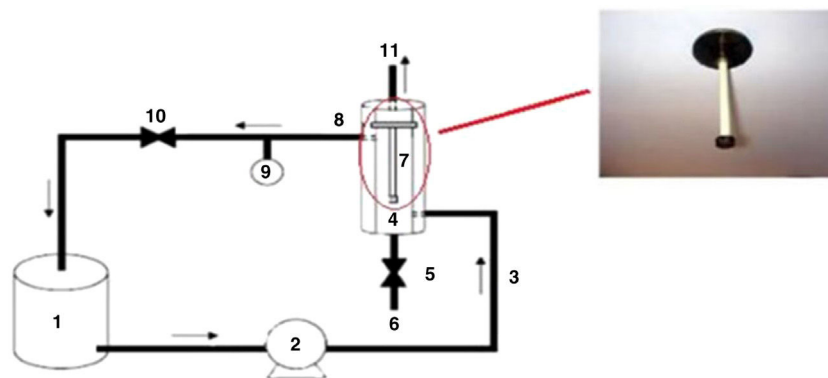


Fig. 1 – Home-made filtration set-up: (1) feed tank, (2) pump, (3) feed stream, (4) membrane module, (5) valve, (6) cleaning channel, (7) membrane, (8) retentate stream, (9) control pressure, (10) valve, (11) permeate stream.

The samples were vertically dried for 24 h at room temperature and then kept for 2 h for sintering at 950 °C with heating and cooling rates of 2 °C/min.

The deposition of the TiO₂ active layer over the two systems was performed using the sol-gel route and the dip-coating method. The sol preparation started by mixing the Tween 80 with isopropanol. Then, acetic acid was added to the solution for the esterification reaction with isopropanol. At last, titanium isopropoxide was added under vigorous stirring and kept stirring for 15 min. The reagents were added according to the molar ratio of 1:45:6:1 for Tween 80:isopropanol:acetic acid:titanium isopropoxide [30]. The amounts were calculated in order to obtain theoretically 0.1 mol of TiO₂, that means we put 0.1:4.5:0.6:0.1 mol of each component mentioned above. Before coating, the samples were thoroughly cleaned with distilled water and acetone using an ultrasound bath and then oven-dried. The identical technique used to deposit the intermediate layer was used to deposit the active layer. The dip-coating procedure was repeated 3 times for the substrate samples and 2 times for the samples of the substrate and intermediate layer. The dipping time for each cycle was fixed at 30 s followed by air drying. After coating, the samples were dried at room temperature for 2 h, calcined with a heating rate of 1 °C/min up to 500 °C, maintained at this temperature for 15 min, then naturally cooled down.

Characterization methods

The range of the thermal study was fixed after a dilatometric analysis using a dilatometer Setsys 16/18 (Setaram, France) with cylindrical samples of 5 mm in diameter and 10 mm in thickness. The adaptability of the sample to extrusion was checked by a plasticity study using two different compositions, (1) C₁: MK50 and 1 wt.% of carboxymethylcellulose (CMC) and (2) C₂: MK50 with 0.6 wt.% of CMC and 0.5 wt.% of polyethylene glycol (PEG). This study was carried out by adopting the Casagrande method which is based on the determination of the Atterberg limits (liquid limit, plastic limit, and plasticity index) [31]. X-ray diffraction (XRD) analysis of the raw materials and mineralogical composition of support samples was performed using Philips X'Pert equipment with Cu K_α radiation. The mercury intrusion porosimeter Autopore II 9215 (Micromeritics, USA) was used to measure the porosity

and average pore diameter of the support samples. The N₂ adsorption-desorption isotherm analysis and application of the BET model were conducted prior to the porosity data of the alumina intermediate layer and the TiO₂ active layer. An Autosorb 1 (Quantachrom, USA) was the tool employed. A universal testing device (Instron, UK) was used to determine the mechanical strength by measuring the resistance to diametrical compression. The measurements were realized on pressed cylindrical samples with a diameter of 5 mm and a thickness of 9 mm. The test was performed with four samples and the average value was reported.

The microstructures of the samples during the preliminary study were analyzed using a Scanning Electron Microscope (SEM) Hitachi Tabletop TM-1000, while the support and supported membrane were followed by a field emission scanning electron microscope (FESEM) Hitachi S-4700.

The membrane performance was evaluated by measuring water flux and dye removal using a homemade set-up (Fig. 1).

The permeation flux (J_w) was determined using Eq. (1):

$$J_w = \frac{V}{A \times t} \quad (1)$$

where V is the volume of permeate collected during the time t , and A is the effective membrane area.

The dye removal study was carried out through filtration studies of an anionic dye (methyl orange) and a cationic dye (malachite green) in the pH of the solutions at a pressure of 4 bar. The removal rate of dye was determined by Eq. (2):

$$R = \frac{C_0 - C_f}{C_0} \times 100 \quad (2)$$

where C_0 and C_f are the dye concentrations before and after filtration, respectively.

Result and discussion

The dilatometric study is important to assign the required temperature range for sintering. The shrinkage and expansion behaviour of the two samples MK25 and MK75 are shown in Fig. 2. The two samples initially shrink, and then expand with a slight difference in their rate. The first shrinkage below

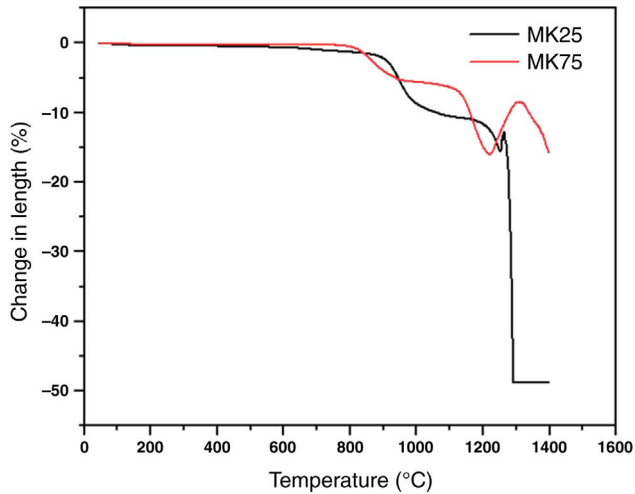


Fig. 2 – Dilatometric curves of MK25 and MK75 compositions.

850 °C corresponds to the dihydroxylation of natural apatite and it's more apparent for MK25. The shrinkage between 850 and 1000 °C is much higher in the MK25 sample and it's related to transformations in the apatite lattice [21]. A further slow shrinkage was observed between 1000 and 1150 °C, indicating

the onset of the vitreous phase formation. Beyond 1180 °C, the two samples showed rapid removal confirming huge densification, and then followed by an intumescent-like expansion as a result of the sample melting. It's worth mentioning that the thermal transformations of MK75 began slightly earlier than those of MK25, which suggests that the metakaolin stimulated the sintering process. To prevent the vitreous phase zone and obtain a porous membrane, the sintering should be performed between 850 and 1000 °C.

Fig. 3 shows the effect of sintering temperature with varying metakaolin amounts on the microstructure of the support samples. The evolution of microstructure is clearly observed after increasing temperature and metakaolin content in the samples. The bonding of grains became more explicit when the temperature progressed from 850 to 1000 °C. Thus, the temperature rise conducted to the formation of more compact microstructures, which are ordinary leading to the amelioration in the mechanical properties [32]. In addition, the role of metakaolin in the sintering activation is more evident in the samples MK50-1000 and MK75-1000. The two samples showed a significant reduction in porosity and the verification area started to appear. These observations were previously mentioned in earlier research [33].

To confirm the SEM micrographs analysis, the effect of sintering temperature on the total porosity and mechanical strength of the different samples was checked, and

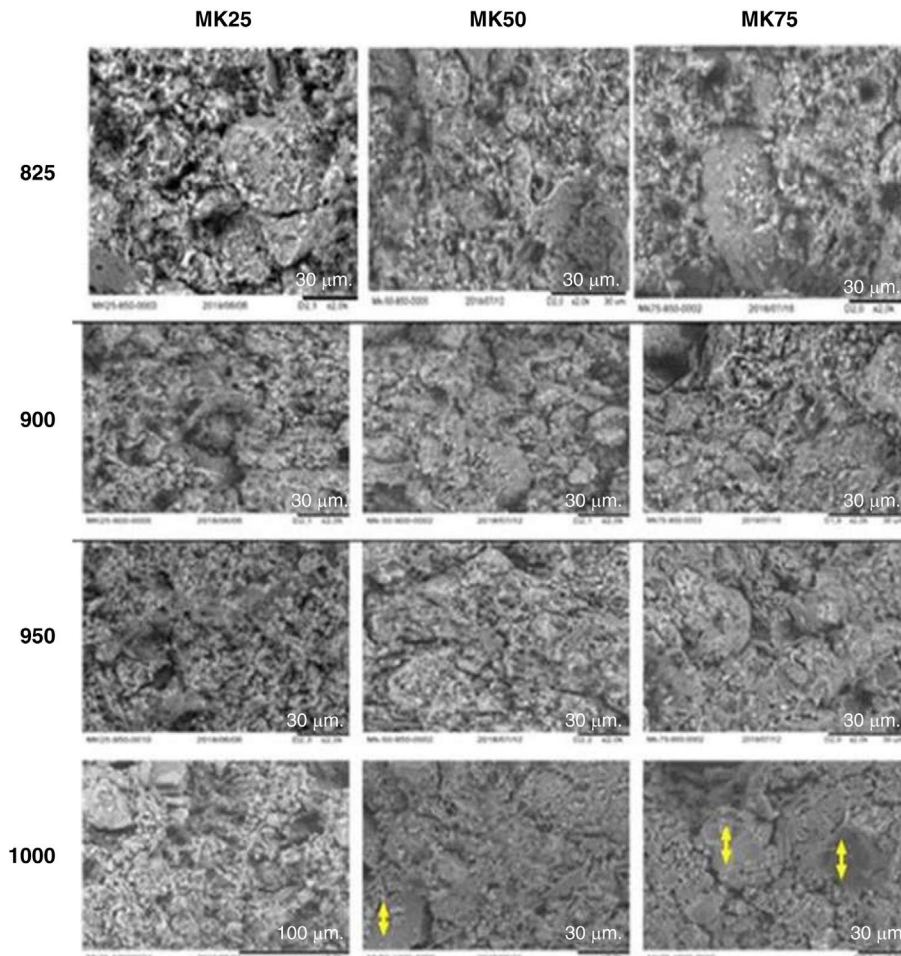


Fig. 3 – SEM images of MK25, MK50, and MK75 samples sintered at different temperatures.

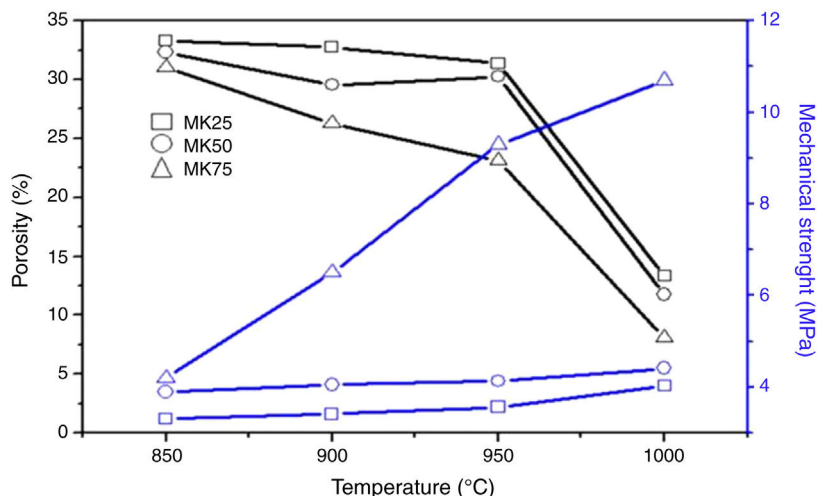


Fig. 4 – Effect of sintering temperature on the compressive strength and porosity of MK25, MK50, and MK75 samples.

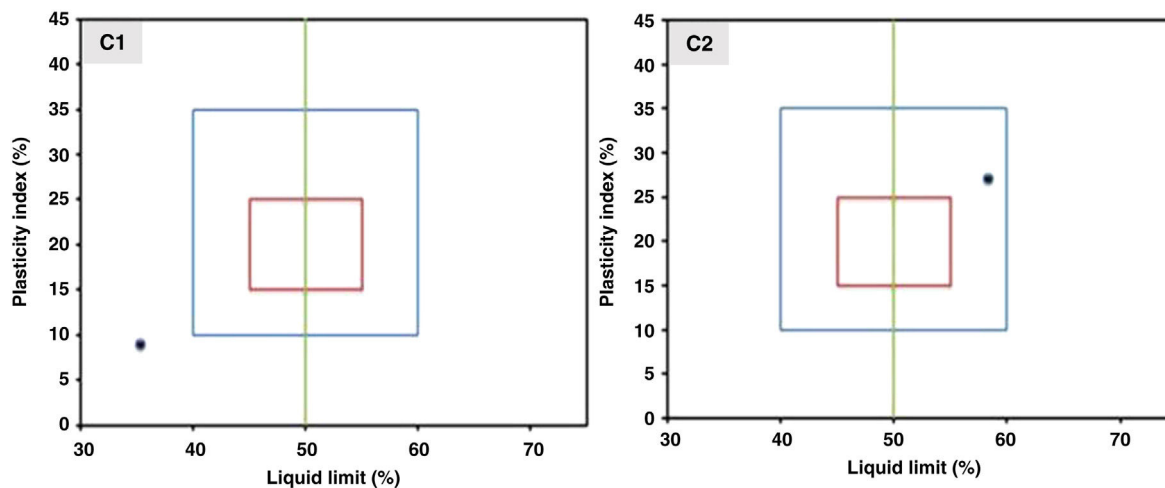


Fig. 5 – Position of C1 and C2 compositions on the workability chart.

the results were summarized in Fig. 4. Unlike the porosity values, the compressive strength of all the samples was improved by increasing the sintering temperature and the metakaolin amount. For instance, when the sintering temperature increased from 850 to 1000 °C, the total porosity of MK25 decreased from 33 to 13% and the compressive strength increased from 1.2 to 4.1 MPa. The overall porosity of MK75 decreased from 30.1 to 8.1%, while the compressive strength increased from 4.2 to 10.7 MPa at the same temperature variation. The existence of a trade-off between porosity and mechanical properties was expected and well-approved in several previous studies [34]. Though, the specimen MK50-950 presents a good compromise between compressive strength and porosity, viz. 4.4 MPa and 30.2%, and consequently was chosen for preparing the membrane support.

The plasticity study was conducted on the inorganic powder mixed with different amounts of carboxymethyl cellulose and polyethylene glycol. In particular, the position of the two compositions C1 and C2 on the workability chart are presented in Fig. 5. According to the position of the coordinate point (liquid limit, plasticity index) on the workability chart, the sample

can be classified as follows: it has a composition with acceptable extrusion properties when the sample falls within the blue diagram, and it has optimal extrusion properties when it falls within the red diagram.

The results show that composition C₂ (inorganic powder mixed with 0.6 wt.% CMC and 0.5 wt.% PEG) presents a coordinate point inside the area with acceptable extrusion properties [31]. Consequently, this composition was decided upon for the extrusion. The support was examined after sintering to determine its crystalline phases, microstructure, porosity, and mechanical strength. The XRD patterns of the powder samples of natural apatite, metakaolin, and the support sample (MK50) are displayed in Fig. 6. In the XRD pattern of the support sample, it can be seen that the typical peaks of natural apatite and metakaolin coexist and no new crystal phases observed at the investigated sintering temperatures.

FESEM provides higher resolution than SEM, reaching the nanoscale, which makes it ideal for imaging extremely fine details of the surface and microstructure of materials. The FESEM images presented in Fig. 7 reveal the porous structure of the support which will have a positive impact on permeabil-

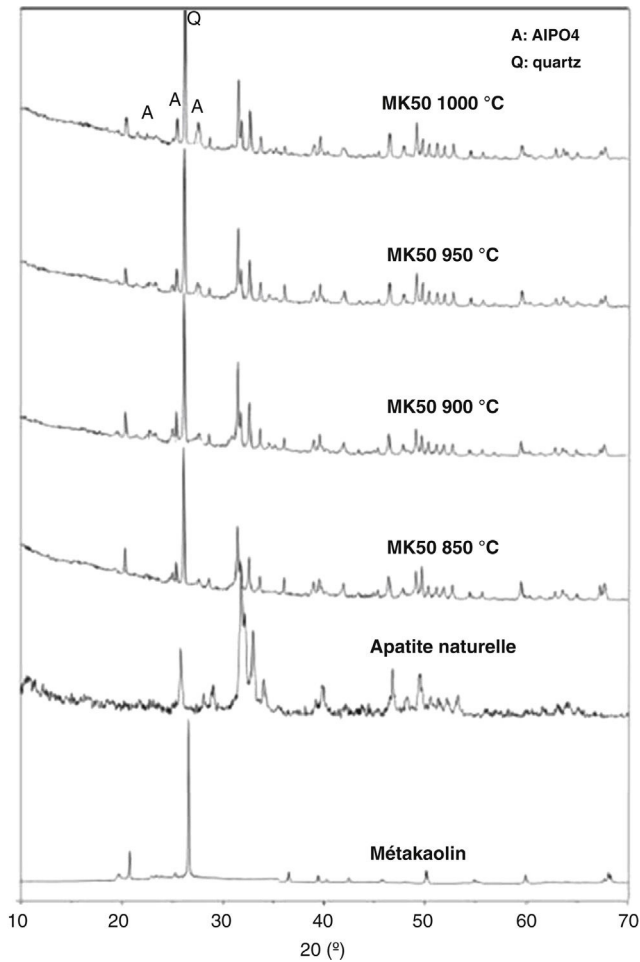


Fig. 6 – XRD pattern of metakaolin, natural apatite, and the MK50 sample sintered at different temperatures.

ity. The high magnification image shows that the pores are well interconnected owing to the neck connection between particles.

Porosity is considered the main factor in the performance of any membrane. Herein, analysis of substrate porosity data obtained through a mercury intrusion porosimeter revealed

a total porosity of 33% and an average pore size of 2.2 μm (Fig. S1). This result seems close to the specimen value found in the preliminary study and is confirming the porous structure shown in FESEM micrographs.

Moreover, it's important to mention that the found compressive strength value of 4.5 MPa is generally acceptable, especially for low-pressure filtration applications, and is similar to previous works [35,36].

After deposition, the morphology and porosity of the intermediate layer were characterized mainly by FESEM and by measuring the medium pore size. The FESEM image of Fig. 8(a) demonstrates that the Al₂O₃ layer was uniformly deposited across the support.

The magnified image (b) reveals the high coalescence of alumina particles which confirms the good sintering. The thickness of the deposited layer was estimated in the order of 50 μm, according to the optical microscope image. Such thickness removes the high rugosity of support, which decreases the risk of cracks after depositing the active layer. Additionally, the findings of the N₂ adsorption-desorption investigation revealed an average pore diameter of less than 30 nm and a BET surface area of about 8.3 m²/g (Table 1).

To achieve the characteristics of a tight UF membrane, the deposition of the TiO₂ thin layer was performed over the two systems as described above. The success and structure of the deposited layer were checked mainly by FESEM, and the results were presented in Figs 9 and 10.

Fig. 9 shows the images of the surface of the active layer deposited directly over the substrate (system 1). As presented in images a and b, it's easy to observe the cracks all over the surface, which means the failure of the coating in this case. The transaction image (C) of the substrate shows the penetration of the nanometric TiO₂ particles inside the large pores (2.2 μm) of the substrate. This suggests that the expanded cracks were mainly due to the porosity gap between the substrate and the active layer.

Fig. 10 shows FESEM pictures for the top-view (a) and cross-section (b–d) of the composite membrane consisting of the TiO₂ active layer coated on the supported intermediate layer (system 2). The top-view image exhibits the homogeneity of the deposited layer without cracks. Image c appears that the UF active layer had a thickness of 2 μm.

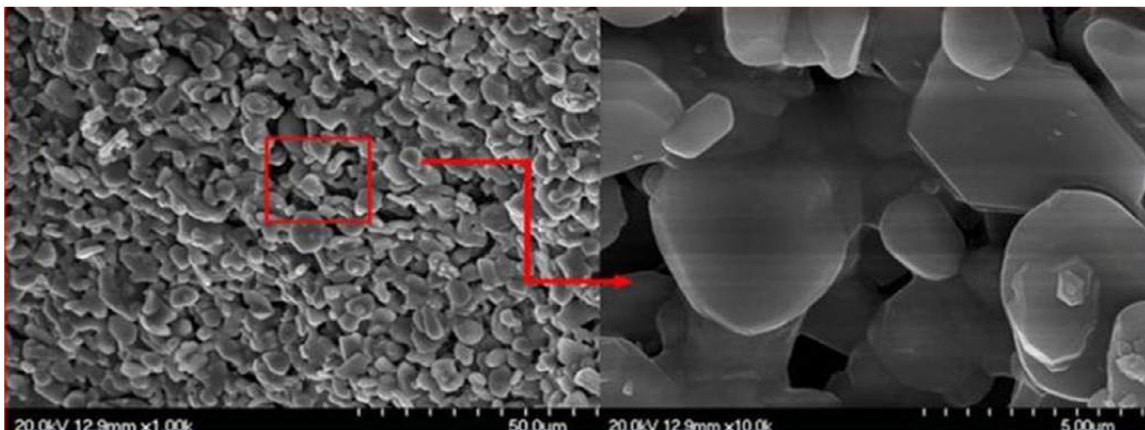


Fig. 7 – FESEM images of MK50 substrate sintered at 950 °C.

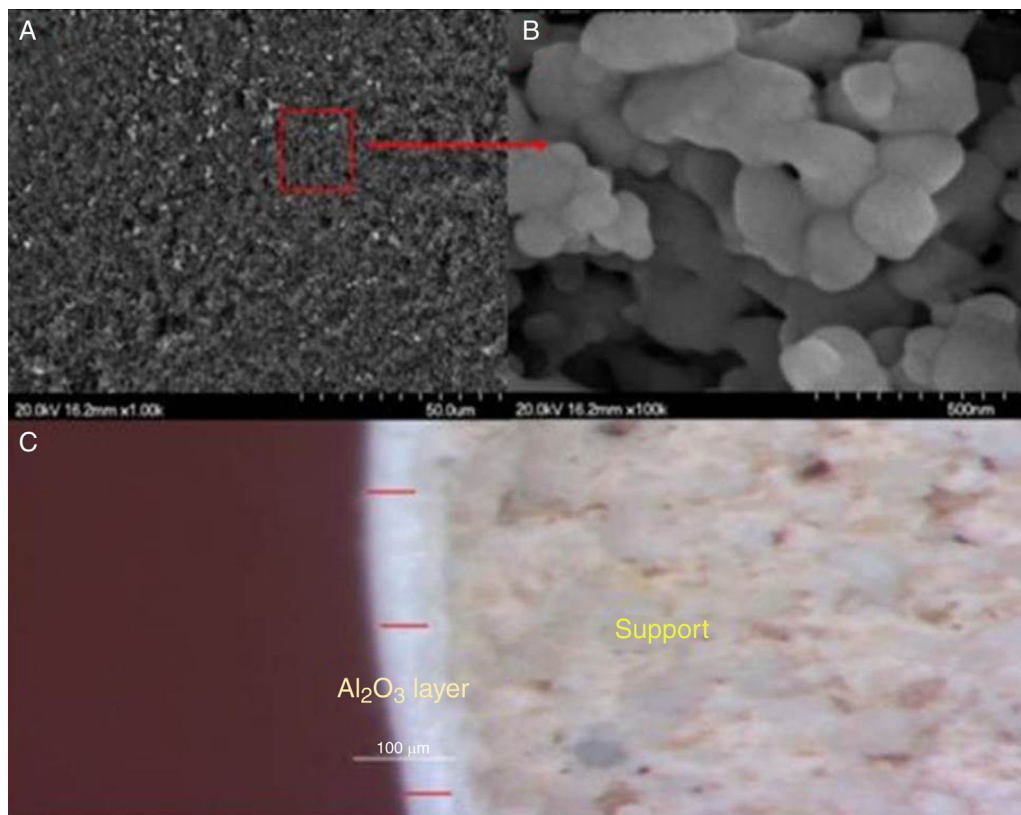


Fig. 8 – FESEM (a and b) and optical microscope (c) images of the alumina deposited layer.

Table 1 – Surface area and average pore diameter of alumina intermediate layer.

BET surface area (m ² /g)	Average pore diameter by BET method (nm)	Average pore diameter by BJH method (nm)
8.3	25.4	29.0

Moreover, image d reveals the high cohesion between the intermediate and the active layer which ensures their stability in case of high running pressure. Accordingly, it can be concluded that the deposition of the TiO₂ active layer is favoured over an intermediate layer.

For further characterization, the TiO₂ active layer was subjected to the adsorption/desorption of the N₂ gas at 77.35 K, and isotherms are presented in Fig. 11.

According to the obtained results, the isotherms shapes correspond to the type IV of the IUPAC isotherms classification [37]. Hence, the TiO₂ active layer displays a mesoporous structure. In addition, the pore size distribution was evaluated using the desorption branch with the BJH (Barrett, Joyner, and Halenda) method, and the result is depicted in Fig. 12. The graph presents one population ranging from 4 to 10 nm and a narrow pore size distribution with a medium pore size of 6.8 nm. This result confirms the mesoporous structure of the prepared membrane which is approaching the nanofiltration range (0.2 nm < average pore size < 2 nm) and belongs to so-called tight ultrafiltration membranes.

The study of water permeability was performed on the support and the supported membrane (system 2), and the results are depicted in Fig. 13. It's obvious the decrease of water flux after the deposition of the intermediate and the active layer

over the substrate, and the permeability shifted from 505.7 to 5.6 L h⁻¹ m⁻² bar⁻¹.

The decline of membrane permeability is the consequence of the graduate porosity, which confers more selectivity to the membrane. In addition, previous studies have reported permeability values approaching the present finding [38].

Ultrafiltration experiments

The ability of the produced membranes to remove cationic and anionic dyes was evaluated. The ultrafiltration experiments were conducted using two synthetic solutions of methyl orange and malachite green with a concentration of 50 mg/L and without altering the pH (Table 2).

The flux variation was followed as a function of time, and the percentages of dye removal were measured after 10 min of filtration. UV-Vis spectroscopy was used to measure the dye concentration. The ultrafiltration membrane showed a high removal rate for the two dyes with a slight superiority of the malachite green (Fig. 14). According to the values reported previously and presented in Table 2 [39,40], the molecular sizes of the two dyes are smaller than the medium pore size of the membrane. Thus, the high rejection rates were realized owing to the polarization layer formed through the hydropho-

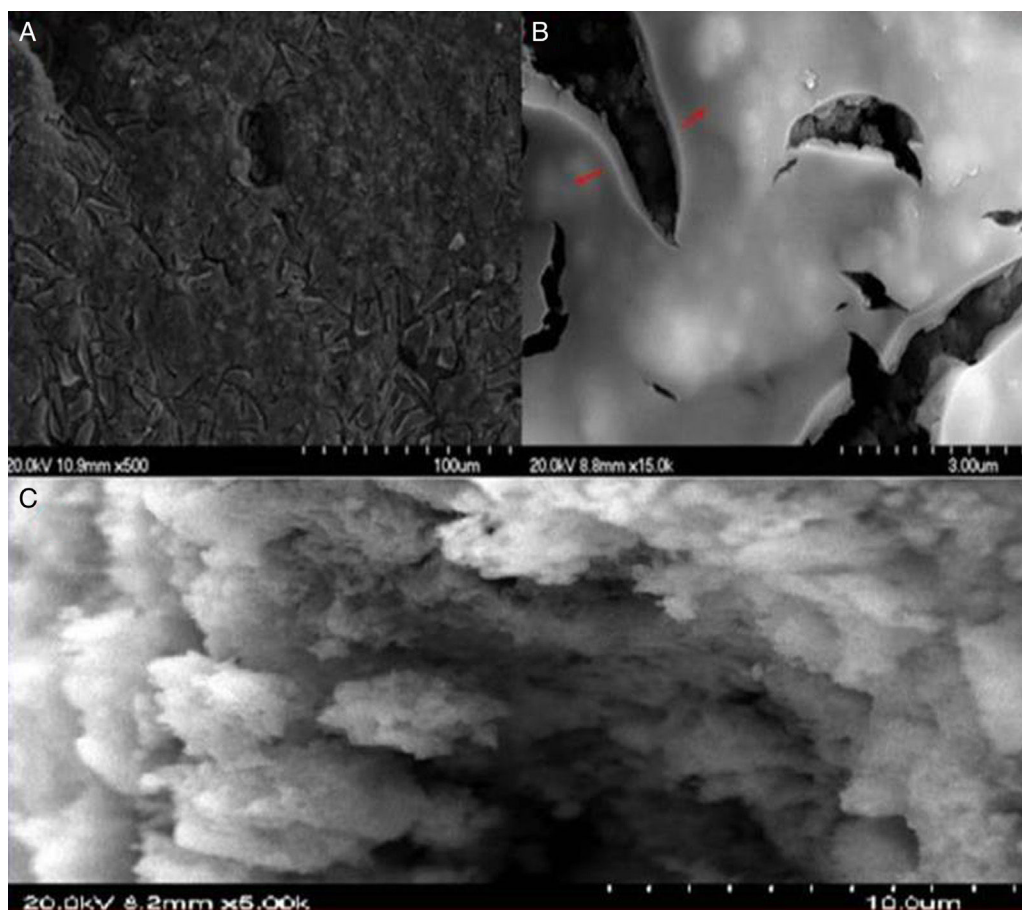


Fig. 9 – FESEM images of the TiO_2 top layer deposited over the MK50 substrate.

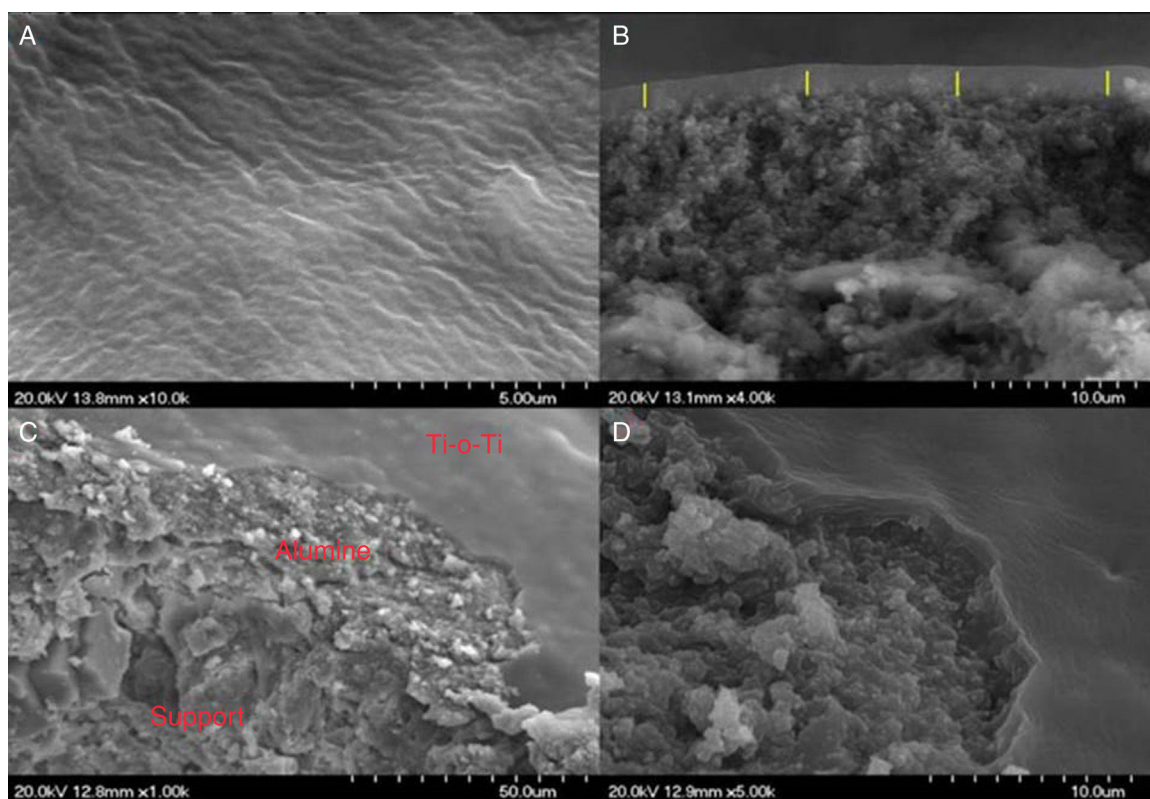


Fig. 10 – FESEM of the TiO_2 top layer deposited over the intermediate layer and MK50 substrate.

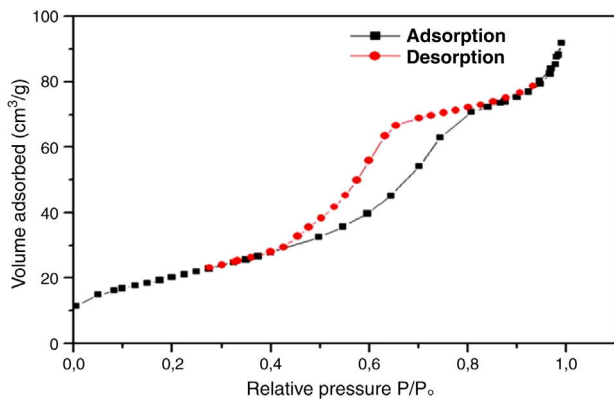


Fig. 11 – N₂ adsorption/desorption isotherms of TiO₂ ultrafiltration membrane.

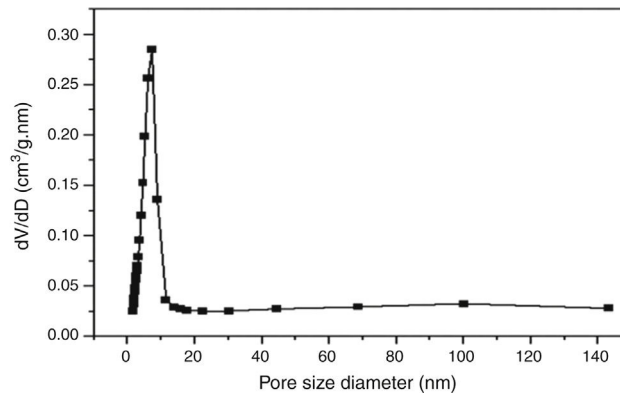


Fig. 12 – Porous size distribution curves of the TiO₂ top layer.

bic interactions between the adjacent aromatic rings of dye molecules [41,42]. Furthermore, it is worth considering that the adsorption of dye molecules onto the membrane surface may also contribute significantly to the overall dye removal

rate. Therefore, the reduction of permeation flux with time is due to the accumulation of the dye layer over the membrane surface (Fig. 14).

Besides, the higher removal rate of the malachite green compared to the methyl orange might be explained by the

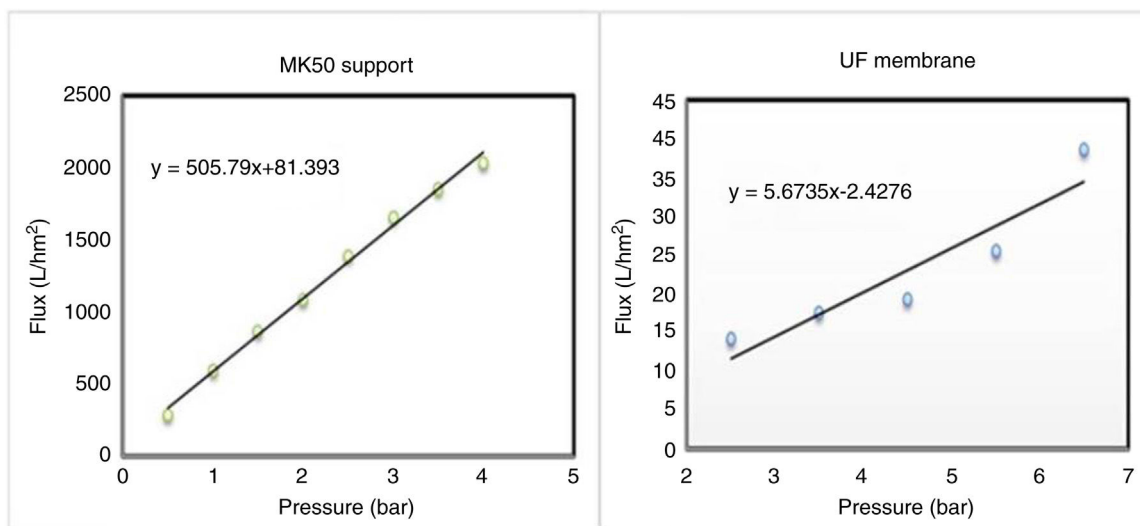
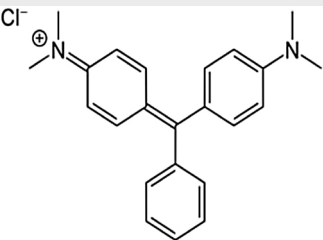
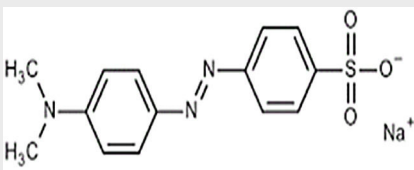


Fig. 13 – Water flux as a function of transmembrane pressure of MK50 support and TiO₂ ultrafiltration membrane.

Table 2 – Characteristics of the used dyes.

	Malachite green	Methyl orange
Molecular structure		
Molecular weight (g/mol)	365	327.33
Maximum wavelength (nm)	625	465
pH	5.4	4.2
Molecular size (nm)	0.8 × 1.58	1.19 × 0.68 × 0.37

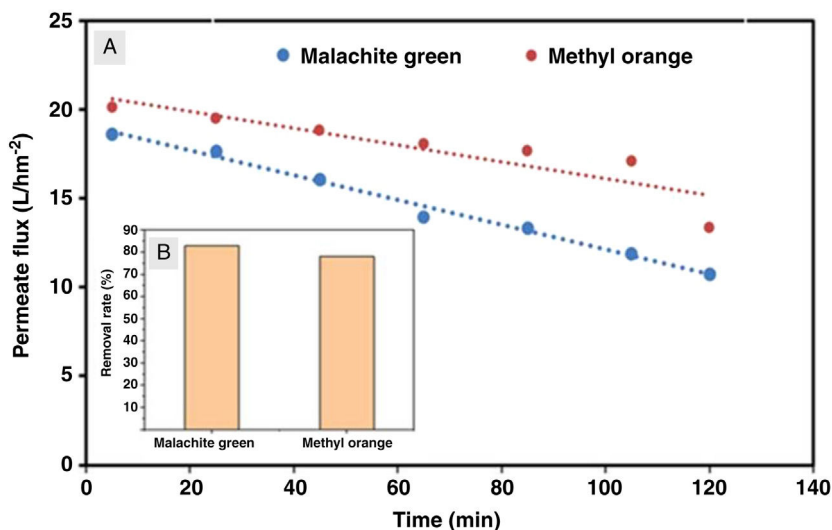


Fig. 14 – Ultrafiltration study: Variation of permeate flux over time (a) and percentage of dye removal (b).

charge interactions between the dye molecules and membrane surface [43]. In this way, Malachite green, which is positively charged, may be repelled by the same charge on the membrane surface, which is more protonated at the solution's pH of 5.4 [44].

The effect of dye concentration on the removal rate was investigated with malachite green. Fig. S2 illustrates the variation of the absorbance of malachite green by increasing the dye concentration. The increase in dye concentration contracted the absorbance values, which implies an increment in the removal rate. This trend is common in the removal of dyes and could be explained by the deposited layer of dyes on the membrane surface acting as an additional filtration barrier [45].

Conclusions

In this work, two novel unconventional materials were used to make inexpensive mesoporous membranes. Three different compositions of natural apatite and metakaolin, namely MK75, MK50, and MK75, were studied at various sintering temperatures to select the suitable composition to make the membrane support. The results showed that metakaolin activated the sintering process, which reduced porosity and enhanced compressive strength. The MK50 specimen sintered at 950 °C had a good compromise between porosity and mechanical resistance and was selected to prepare the support. The deposition of the TiO₂ mesoporous top layer was favoured over an intermediate layer of alumina. The prepared membrane revealed a medium pore size of 6.8 nm and water permeability of 5.6 L h⁻¹ m⁻² bar⁻¹. The ultrafiltration experiments have shown a high removal rate for cationic and anionic dyes with removal rates above 75% without adjusting the pH. Further research using suitable setups to harness the TiO₂ layer's photocatalytic properties could greatly improve dye removal and wastewater treatment effectiveness.

Appendix A. Supplementary data

Supplementary data associated with this article can be found, in the online version, at [doi:10.1016/j.bsevcv.2023.10.002](https://doi.org/10.1016/j.bsevcv.2023.10.002).

REFERENCES

- [1] I.M. Ibraheem, G.M. El-Qady, A. ElGalladi, Hydrogeophysical and structural investigation using VES and TDEM data: a case study at El-Nubariya–Wadi El-Natron area, west Nile Delta, Egypt, *NRIAG J. Astron. Geophys.* 5 (2016) 198–215, <http://dx.doi.org/10.1016/J.NRJAG.2016.04.004>.
- [2] A. Rafiq, M. Ikram, S. Ali, F. Niaz, M. Khan, Q. Khan, M. Maqbool, Photocatalytic degradation of dyes using semiconductor photocatalysts to clean industrial water pollution, *J. Ind. Eng. Chem.* 97 (2021) 111–128, <http://dx.doi.org/10.1016/J.JIEC.2021.02.017>.
- [3] Y. Guesmi, H. Agougui, R. Lafi, M. Jabli, A. Hafiane, Synthesis of hydroxyapatite-sodium alginate via a co-precipitation technique for efficient adsorption of Methylene Blue dye, *J. Mol. Liq.* 249 (2018), <http://dx.doi.org/10.1016/j.molliq.2017.11.113>.
- [4] F. Ruscasso, I. Cavello, G. Curutchet, S. Cavalitto, Antarctic yeasts: potential use in a biologic treatment of textile azo dyes (n.d.). <https://doi.org/10.1186/s40643-022-00507-5>.
- [5] C. Castel, E. Favre, Membrane separations and energy efficiency, *J. Membr. Sci.* 548 (2018) 345–357, <http://dx.doi.org/10.1016/J.MEMSCI.2017.11.035>.
- [6] Z. Maletskyi, Advances in membrane materials and processes for water and wastewater treatment, UTC (2022), <http://dx.doi.org/10.1021/bk-2020-1348.ch001>.
- [7] S.K. Hubadillah, M.R. Jamalludin, M.H. Dzarfan Othman, Y. Iwamoto, Recent progress on low-cost ceramic membrane for water and wastewater treatment, *Ceram. Int.* (2022), <http://dx.doi.org/10.1016/J.CERAMINT.2022.05.255>.
- [8] Y. Dong, H. Wu, F. Yang, S. Gray, Cost and efficiency perspectives of ceramic membranes for water treatment, *Water Res.* 220 (2022) 118629, <http://dx.doi.org/10.1016/J.WATRES.2022.118629>.

- [9] S.L. Sandhya Rani, R.V. Kumar, Insights on applications of low-cost ceramic membranes in wastewater treatment: a mini-review, *Case Stud. Chem. Environ. Eng.* 4 (2021) 100149, <http://dx.doi.org/10.1016/j.csee.2021.100149>.
- [10] D. Liang, J. Huang, Y. Zhang, Z. Zhang, H. Chen, H. Zhang, Influence of dextrin content and sintering temperature on the properties of coal fly ash-based tubular ceramic membrane for flue gas moisture recovery, *J. Eur. Ceram. Soc.* 41 (2021) 5696–5710, <http://dx.doi.org/10.1016/j.jeurceramsoc.2021.04.055>.
- [11] I. Hedfi, N. Hamdi, M.A. Rodriguez, E. Srasra, Development of a low cost micro-porous ceramic membrane from kaolin and alumina, using the lignite as porogen agent, *Ceram. Int.* 42 (2016) 5089–5093, <http://dx.doi.org/10.1016/j.ceramint.2015.12.023>.
- [12] M. Mouiya, A. Bouazizi, A. Abourriche, A. Benhammou, Y. El Hafiane, M. Ouammou, Y. Abouliatim, S.A. Younssi, A. Smith, H. Hannache, Fabrication and characterization of a ceramic membrane from clay and banana peel powder: application to industrial wastewater treatment, *Mater. Chem. Phys.* 227 (2019) 291–301, <http://dx.doi.org/10.1016/j.matchemphys.2019.02.011>.
- [13] D. Rashad, S.K. Amin, M.S. Mansour, H. Abdallah, Fabrication of low-cost antibacterial microfiltration tubular ceramic membranes, *Ceram. Int.* 48 (2022) 11489–11501, <http://dx.doi.org/10.1016/j.ceramint.2022.01.005>.
- [14] K.P. Goswami, K. Pakshirajan, G. Pugazhenthii, Process intensification through waste fly ash conversion and application as ceramic membranes: a review, *Sci. Total Environ.* 808 (2022), <http://dx.doi.org/10.1016/j.scitotenv.2021.151968>.
- [15] S.L. Sandhya Rani, R.V. Kumar, Insights on applications of low-cost ceramic membranes in wastewater treatment: a mini-review, *Case Stud. Chem. Environ. Eng.* 4 (2021) 100149, <http://dx.doi.org/10.1016/j.csee.2021.100149>.
- [16] A. Abdullayev, M.F. Bekheet, D.A.H. Hanaor, A. Gurlo, Materials and applications for low-cost ceramic membranes, *Membranes (Basel)* 9 (2019), <http://dx.doi.org/10.3390/membranes9090105>.
- [17] P.T.P. Aryanti, A.N. Hakim, S. Widodo, I.N. Widiassa, I.G. Wenten, Prospect and challenges of tight ultrafiltration membrane in drinking water treatment, in: *IOP Conf Ser Mater Sci Eng*, Institute of Physics Publishing, 2018, <http://dx.doi.org/10.1088/1757-899X/395/1/012012>.
- [18] M. Hu, S. Yang, X. Liu, R. Tao, Z. Cui, C. Matindi, W. Shi, R. Chu, X. Ma, K. Fang, M. Titus, B.B. Mamba, J. Li, Selective separation of dye and salt by PES/SPSF tight ultrafiltration membrane: roles of size sieving and charge effect, *Sep. Purif. Technol.* 266 (2021), <http://dx.doi.org/10.1016/j.seppur.2021.118587>.
- [19] E.S. Mansor, E.A. Ali, A.M. Shaban, Tight ultrafiltration polyethersulfone membrane for cheese whey wastewater treatment, *Chem. Eng. J.* 407 (2021), <http://dx.doi.org/10.1016/j.cej.2020.127175>.
- [20] S. Fang, X. Shi, X. Wang, Z. Zhang, C. Yin, Z. Zhang, T. Ju, S. Xiong, Y. Wang, Large-pore covalent organic frameworks for ultra-fast tight ultrafiltration (TUF), *J. Membr. Sci.* 637 (2021), <http://dx.doi.org/10.1016/j.memsci.2021.119635>.
- [21] Y. Guesmi, R. Lafi, H. Agougui, M. Jabli, A. Oun, S. Majumdar, A. Hafiane, Synthesis and characterization of alpha alumina-natural apatite based porous ceramic support for filtration application, *Mater. Chem. Phys.* 239 (2020) 122067, <http://dx.doi.org/10.1016/j.matchemphys.2019.122067>.
- [22] J. Karuppaiyan, R. Jeyalakshmi, S. Kiruthika, M.A. Wadaan, M.F. Khan, W. Kim, A study on the role of surface functional groups of metakaolin in the removal of methylene blue: characterization, kinetics, modeling and RSM optimization, *Environ. Res.* 226 (2023) 115604, <http://dx.doi.org/10.1016/j.envres.2023.115604>.
- [23] N. Lertcumfu, P. Jaita, G. Rujijanagul, T. Tunkasiri, Characterization of metakaolin-based materials for dye adsorption from aqueous solution, *Solid State Phenom.* 283 (2018) 88–94, <http://dx.doi.org/10.4028/www.scientific.net/SSP.283.88>.
- [24] P. Jantawasu, T. Sreethawong, S. Chavadej, Photocatalytic activity of nanocrystalline mesoporous-assembled TiO₂ photocatalyst for degradation of methyl orange monoazo dye in aqueous wastewater, *Chem. Eng. J.* 155 (2009) 223–233, <http://dx.doi.org/10.1016/j.cej.2009.07.036>.
- [25] C.K.C.T.N. Prabhu, R.R.S. Kiran, R.H. Krishna, Applications of artificial neural network and Box-Behnken Design for modelling malachite green dye degradation from textile effluents using TiO₂ photocatalyst, *Environ. Eng. Res.* 27 (2021) 200553–200560, <http://dx.doi.org/10.4491/eeer.2020.553>.
- [26] N. Setthaya, P. Chindaprasit, S. Yin, K. Pimraksa, TiO₂-zeolite photocatalysts made of metakaolin and rice husk ash for removal of methylene blue dye, *Powder Technol.* 313 (2017) 417–426, <http://dx.doi.org/10.1016/j.powtec.2017.01.014>.
- [27] H. Tan, Y. Zhang, B. Li, H. Yang, H. Hou, Q. Huang, Preparation of TiO₂-coated glass flat membrane and its photocatalytic degradation of methylene blue, *Ceram. Int.* 49 (2023) 17236–17244, <http://dx.doi.org/10.1016/j.ceramint.2023.02.089>.
- [28] Y. Zhang, H. Tan, C. Wang, B. Li, H. Yang, H. Hou, C. Xiao, TiO₂-coated glass hollow fiber membranes: preparation and application for photocatalytic methylene blue removal, *J. Eur. Ceram. Soc.* 42 (2022) 2496–2504, <http://dx.doi.org/10.1016/j.jeurceramsoc.2021.12.075>.
- [29] M. Khabbouchi, K. Hosni, M. Mezni, C. Zanelli, M. Doggy, M. Dondi, E. Srasra, Interaction of metakaolin-phosphoric acid and their structural evolution at high temperature, *Appl. Clay Sci.* 146 (2017) 510–516, <http://dx.doi.org/10.1016/j.clay.2017.07.006>.
- [30] H. Choi, E. Stathatos, D.D. Dionysiou, Sol-gel preparation of mesoporous photocatalytic TiO₂ films and TiO₂/Al₂O₃ composite membranes for environmental applications, *Appl. Catal. B* 63 (2006) 60–67, <http://dx.doi.org/10.1016/j.apcat.2005.09.012>.
- [31] I. Hedfi, N. Hamdi, M.A. Rodriguez, E. Srasra, Development of a low cost micro-porous ceramic membrane from kaolin and alumina, using the lignite as porogen agent, *Ceram. Int.* 42 (2016) 5089–5093, <http://dx.doi.org/10.1016/j.ceramint.2015.12.023>.
- [32] J. Malzbender, Mechanical aspects of ceramic membrane materials, *Ceram. Int.* 42 (2016) 7899–7911, <http://dx.doi.org/10.1016/j.ceramint.2016.02.136>.
- [33] D.O. Obada, D. Dodoo-Arhin, M. Dauda, F.O. Anafi, A.S. Ahmed, O.A. Ajayi, The impact of kaolin dehydroxylation on the porosity and mechanical integrity of kaolin based ceramics using different pore formers, *Results Phys.* 7 (2017) 2718–2727, <http://dx.doi.org/10.1016/j.rinp.2017.07.048>.
- [34] Q. Gu, M. Kotobuki, C.H. Kirk, M. He, G.J.H. Lim, T.C.A. Ng, L. Zhang, H.Y. Ng, J. Wang, Overcoming the trade-off between water permeation and mechanical strength of ceramic membrane supports by interfacial engineering, *ACS Appl. Mater. Interfaces* 13 (2021) 29199–29211, <https://doi.org/10.1021/ACSAMI.1C08157/ASSET/IMAGES/LARGE/AM1C08157.0007.JPEG>.
- [35] C.F. Li, S.H. Zhong, Kieselguhr-Mullite ceramic membrane substrate fabricated by line compounding technique, *J. Membr. Sci.* 204 (2002) 89–95, [http://dx.doi.org/10.1016/S0376-7388\(02\)00019-4](http://dx.doi.org/10.1016/S0376-7388(02)00019-4).
- [36] J. bin Zhu, H. Yan, Microstructure and properties of mullite-based porous ceramics produced from coal fly ash

- with added Al₂O₃, *Int. J. Miner. Metall. Mater.* 24 (2017) 309–315, <http://dx.doi.org/10.1007/S12613-017-1409-2>.
- [37] M. Muttakin, S. Mitra, K. Thu, K. Ito, B.B. Saha, Theoretical framework to evaluate minimum desorption temperature for IUPAC classified adsorption isotherms, *Int. J. Heat Mass Transf.* 122 (2018) 795–805, <http://dx.doi.org/10.1016/J.IJHEATMASSTRANSFER.2018.01.107>.
- [38] X. Ma, P. Chen, M. Zhou, Z. Zhong, F. Zhang, W. Xing, Tight ultrafiltration ceramic membrane for separation of dyes and mixed salts (both NaCl/Na₂SO₄) in textile wastewater treatment, *Ind. Eng. Chem. Res.* 56 (2017) 7070–7079, <https://doi.org/10.1021/ACS.IECR.7B01440/ASSET/IMAGES/MEDIUM/IE-2017-01440C.0011.GIF>.
- [39] J. Huang, Molecular sieving effect of a novel hyper-cross-linked resin, *Chem. Eng. J.* 165 (2010) 265–272, <http://dx.doi.org/10.1016/j.cej.2010.09.028>.
- [40] N.B. Swan, M.A.A. Zaini, Adsorption of malachite green and congo red dyes from water: recent progress and future outlook, *Ecol. Chem. Eng. S* 26 (2019) 119–132, <http://dx.doi.org/10.1515/eces-2019-0009>.
- [41] X. Zhang, Selective separation membranes for fractionating organics and salts for industrial wastewater treatment: design strategies and process assessment, *J. Membr. Sci.* 643 (2022) 120052, <http://dx.doi.org/10.1016/J.MEMSCI.2021.120052>.
- [42] S. Gholami, J.L. Llacuna, V. Vatanpour, A. Dehqan, S. Paziresh, J.L. Cortina, Impact of a new functionalization of multiwalled carbon nanotubes on antifouling and permeability of PVDF nanocomposite membranes for dye wastewater treatment, *Chemosphere* 294 (2022) 133699, <http://dx.doi.org/10.1016/J.CHEMOSPHERE.2022.133699>.
- [43] S. Kim, M. Yu, Y. Yoon, Fouling and retention mechanisms of selected cationic and anionic dyes in a Ti₃C₂T_x MXene-ultrafiltration hybrid system, *ACS Appl. Mater. Interfaces* 12 (2020) 16557–16565, <http://dx.doi.org/10.1021/acsami.0c02454>.
- [44] A. Bouazizi, M. Breida, B. Achiou, M. Ouammou, J.I. Calvo, A. Aaddane, S.A. Younssi, Removal of dyes by a new nano-TiO₂ ultrafiltration membrane deposited on low-cost support prepared from natural Moroccan bentonite, *Appl. Clay Sci.* 149 (2017) 127–135, <http://dx.doi.org/10.1016/j.clay.2017.08.019>.
- [45] A. Chougui, K. Zaiter, A. Belouatek, B. Asli, Heavy metals and color retention by a synthesized inorganic membrane, *Arab. J. Chem.* 7 (2014) 817–822, <http://dx.doi.org/10.1016/j.arabjc.2012.11.017>.